Research on Chemical Intermediates
https://doi.org/10.1007/s11164-020-04297-3

A novel method for the synthesis and characterization of 10-hexyl-3-(1-hexyl-4, 5-diphenyl-1H-imidazol-2-yl)-10H-phenothiazine: DFT computational, in vitro anticancer and in silico molecular docking studies

J. Irshad Ahamed, et al. ***[full author details at the end of the article]***

Received: 14 August 2020 / Accepted: 8 October 2020

Abstract

This study aimed to newly synthesized compound 10-hexyl-3-(1-hexyl-4, 5-diphenyl-1H-imidazol-2-yl)-10H-phenothiazine (abbreviated as HHDIP) by direct and thermal condensation methods, which were characterized by different spectral analysis. The optimized geometry completed the theoretical calculation; the Fourier-transform infrared spectroscopy (FTIR) vibrational frequency studies of HHDIP were found by using the (density functional theory) ab initio calculation with B3LYP/6-311++G (d,p) level. The computed and scaled vibrational frequency values were well matched with the experimental FTIR and Fourier-transform Raman spectroscopy (FT-Raman) spectra. A particular understanding of the FTIR spectra of this title compound was performed by the computed potential energy distribution. The UV–Vis, ^{1}H, and ^{13}C NMR investigations were completed as well as observed; these theoretical outcomes have been seen as in good concurrence with the experimental value. The mass spectroscopy investigation was completed to this compound. In addition to this title compound, the computed (HOMO and LUMO) energy values have been revealed with the charge transfer inside the organic molecules. Nonlinear optics and Mulliken population studies were completed for this title compound. Finally, intensive studies on their anticancer properties were studied through in vitro as well as in silico approaches, suggesting our title compound exhibited tremendous anticancer activity at the concentration value of 250 µg/mL. The in silico docking and adsorption, distribution, metabolisms, excretion and toxicity (ADMET) studies were executed through commercial docking software Discovery Studio, version 4.0 against the protein target c-Met kinase (hepatocyte growth factor; PDB ID: 3F66). The results showed a ligand–receptor interaction energy value of − 64.494 KCal/mol against 3F66 protein (standard anticancer drug tivantinib exhibited − 57.804 KCal/

Electronic supplementary material The online version of this article (https://doi.org/10.1007/s11164-020-04297-3) contains supplementary material, which is available to authorized users.

Published online: 23 October 2020

mol). In the ADMET study, it gives good results of nonmutagenic and noncarcinogenic activities. However, in vitro studies exposed more significant antioxidant activity at the range of hydrogen peroxide (H_2O_2) scavenging activity as 66.31% and 52.877% which showed a vigorous DPPH radical scavenging antioxidant activity concentration value of 500 µg/mL. Further studies are desired to explore its promising anticancer, clinical research and other pharmacological aspects.

Keywords Synthesis of new HHDIP · Spectroscopic analysis · DFT computational · Anticancer · Molecular docking

Introduction

Nowadays, chemotherapy is routinely applied to treat the cancer disease although it has different kinds of toxicities such as myelotoxicity, cardiotoxicity, renal toxicity and pulmonary toxicity. These side effects create serious health problems and sometimes lead to death. Cancer is yet a life-threatening disease due to a lack of effective anticancer drugs and the side effects of chemotherapy [1]. Therefore, efforts are still being needed to develop high-active anticancer agents for the successful treatment for cancer. Heterocyclic class of the chemical compound works for a vital function in modern drug discovery by a structural modification to prepare several compounds. The imidazole-containing compounds have several biological activities as well as pharmaceutical significance with anti-HIV, antidiabetic and antimalarial activities [2–8]. Imidazole products are illustrated to be pharmacologically and physiologically active that are utilized in the treatment for various diseases. Its portion-containing compounds are obtained to be a great number of novel chemotherapeutic materials based on imidazole nucleus, natural products, clinical active molecules, and several medicines possess the imidazole ring, comprising ketoconazole utilized for the treatment for bacterial infections, gastric ulcers and fungal infections [9–11]. The search of a new imidazole agent for the cure of cancer is an essential tool in medicinal chemistry [12]. A new acidic ionic liquid (AIL) based on imidazolium cations is used as a catalyst for the one-pot synthesis of 2-aryl- 1H-phenanthro[9,10-d]imidazole derivatives [13]. The 1,2,4,5-tetrasubstituted imidazole derivatives have shown enhanced anticancer and antibacterial activities against Huh-7 hepatocellular carcinoma cell and four bacterial species names such as wild-type *Escherichia coli*, wild-type *Staphylococcus aureus*, *Pseudomonas aeruginosa* PAM1032, and *Escherichia coli*-NMD-1 [14]. The preparation of chalcones-imidazole (E)-1-(4-((1H-imidazol-1-yl) methyl) phenyl)-3-phenylprop-2-en-1-one derivatives has exhibited superior antibacterial and antifungal activities [15]. Benzimidazole derivatives have shown superior antiviral and anticancer biological activities [16]. A series of 1-(2-(4-morpholinomethyl)-1H-benzoimidazol-1-yl)propan-2-one oxime-ethers has excellent antifungal activities [17]. The syntheses of these heterocyclic compounds are cost-effective, and their initial materials are readily available. Owing to their significance, they have become a suitable goal for synthetic and clinical uses. The newly synthesized compound of HHDIP has performed the different spectroscopic

analyses by using experimental and theoretical density functional theory (DFT) calculation with B3LYP/6-311 ++G (d,p) level. Furthermore, in vitro and in silico methods have been done against cancer studies; it was well known to act as an effective agent of anticancer in this present work.

Materials and methods

Chemicals and Reagents

The following chemicals and reagents such as benzil, phenothiazine, n-bromohexane (Sigma-Aldrich, USA), Silica gel with a mesh of 60–120 (Merck, India), precoated aluminum sheet of silica gel G/UV-254 of 0.2 mm thickness (Merck, Germany), K_2CO_3, hexane-1-amine, NH_4OAC, ethyl alcohol, methanol, CH_3COOH, $POCl_3$, EtOAc, Na_2SO_4 and sodium hydroxide (Spectrochem, India) were utilized for the synthesis of imidazole compound.

Spectral characterization

The title compound was recorded by infrared (IR), ^1H and ^{13}C (NMR—nuclear magnetic resonance) data information, and its melting point was found by a superfit (India) capillary melting-point apparatus. The title molecule IR spectrum was accomplished on a Perkin Elmer spectrometer V 10.03.06 utilizing the potassium bromide (KBr) disk, and FT-Raman spectrum was also completed in 4000–100 cm^{-1} range on BRUCKER RFS 27 utilizing Nd:YAG laser (excitation wavelength) with the resolution of 2 cm^{-1} at SAIF, IIT, Chennai. The UV–Vis: λmax spectrum of compounds was recorded using Shimadzu UV–Vis spectrometer. The ^{1}HNMR spectra were confirmed on a Bruker Avance (400 MHz) spectrometer in Chloroform-D ($CDCl_3$) solvent, and chemical shift values were confirmed in units δ (ppm) relative to tetramethylsilane (Me4Si) as an internal standard. ^{13}C-NMR spectra were confirmed at 100 MHz in $CDCl_3$ with the same internal standard. The mass spectra were performed on Total Ion Current (TIC) Chromatogram spectrometers. Elemental analyses were executed on 2400 Series II PerkinElmer CHNS/O Elemental Analyzer (India). Elemental (CHNS/O) analysis specified that the calculated and found values were within the acceptable limits (±0.4%). Reactions were observed by means of TLC utilizing precoated plates (Merck, India). Column chromatographic separation was done by silica gel with a mesh of 60–120.

Synthesis of HHDIP

The 10-hexyl-10H-phenothiazine-3-carbaldehyde (1 g, 3.2 mmol), benzil (0.6 g, 3.2 mmol), hexan-1-amine (0.3 g, 0.0032 mmol) and ammonium acetate (NH_4OAc) (0.4 g, 8 mmol) were mixed to a 100 mL RB flask, and 20 mL of acetic acid (CH_3COOH) was added to this reaction mixture. The reaction was refluxed at 70–90 °C for 3 h. The improvement in the final reaction was monitored by TLC.

After the reaction ended, the crude mass was permitted to be purified by 60–120 mesh column chromatography techniques using the mixture of 40% of hexane/EtOAc as eluent.

Experimental data

Yield: 95%; brown solid; mp:523–524 °C; IR (KBr, ν, cm^{-1}): 3325, 2974, 2881, 1654, 1379,, 1328, 1274, 1087, 1045, 879, 802, 605; (FT-Raman, ν, cm^{-1}); 3239, 3118, 3034, 1667, 1604, 1563, 1509, 1435, 1279, 1038, 984; UV–Vis: λmax 364 nm;^{1}H NMR (400 MHz, $CDCl_3$): δ 0.74–0.70 (t, $J = 6.9$ Hz, 3H), 0.86–0.89 (m, 3H), 0.94–0.99 (m, 4H), 1.03–1.08 (m, 2H), 1.291.32(m, 6H), 1.33–1.48(m, 2H), 1.78–1.86(m, 2H), 3.82–3.89 (m, 4H), 6.88–6.94 (m, 3H), 7.09–7.20 (m, 5H), 7.38–7.51 (m, 9H); ^{13}C NMR (100 MHz, $CDCl_3$): 13.82, 13.99, 22.23, 22.60, 25.89, 26.59, 26.80, 30.36, 30.81, 31.45, 44.76, 47.76, 115.16, 115.46, 122.59, 124.48, 125.16, 126.17, 126.83, 127.47, 127.82, 128.01, 128.11, 128.58, 129.00, 129.03, 129.56, 129.92, 131.05, 131.61, 134.57, 144.91, 145.65, 146.87; Analysis calcd. % for $C_{39}H_{43}N_3S$: C, 79.96; H, 7.40; N, 7.17; S, 5.47; Found %: C, 79.84; H, 7.34; N, 7.03; S, 5.32; MS (ESI) for $C_{39}H_{43}N_3S$: *m/z* 586.60 $[M+H]^+$.

Computational details

The DFT-optimized geometry of the HHDIP was computed by B3LYP (Beckee-3-Lee–Yang–Parr) method, Gaussian 09 program package as well as included 6-311++G (d,p) basis set [18–21]. In DFT study, the ab initio method of molecular calculating properties has recently enhanced [22–24]. The optimized structural parameters were utilized for simulating vibrational frequencies, and their frequency assignments were completed accurately through VEDA program. To find visual animation and to perform verification of the (normal modes) assignment, Gauss View program [25] has been utilized. The (FMOs—Frontier molecular orbitals) energies, molecular optimization structure, bond parameters, Mulliken population analyses, NLO, thermodynamic studies have been completed by DFT method. Electronic properties were completed by DFT time-dependent (TD-DFT) methods [26–28]. Proton ^{1}H and carbon^{13}C NMR spectra results were completed, and molecules chemical shifts were computed using (GIAO—gauge-independent atomic orbital) method [29].

In vitro anticancer activity

The liver cancer (HepG2) cell line was used to check the anticancer activity of the compound HHDIP. Cells were cultured and conserved in Minimal Essential Media (MEM) (Hi-Media, India) enhanced with 10% fetal bovine serum (FBS) Cistron Laboratories), Trypsin, MTT (methyl thiazolyl diphenyl-tetrazolium bromide) and dimethyl sulfoxide (DMSO) HiMedia, India). Cells were incubated at 37 °C in a 5% CO_2 atmosphere; they were regularly subcultured and preserved in 2% MEM. A confluent monolayer of HepG2 cells was trypsinized and suspended in 10% MEM;

100 µL of cells suspension was transferred to 96 well plates, and 10% MEM was added as well as the plate incubated at 37 °C at 5% CO_2 environment. Various concentrations of compounds were prepared as 100 µg/mL, 50 µg/mL, 25 µg/mL, 12.5 µg/mL, 6.25 µg/mL, 3.125 µg/mL, 1.56 µg/mL and 0.78 µg/mL and transferred in 96 well plates, and finally 100 µL of 2% MEM was added. Morphological alterations of the HepG2 cells were monitored every 24 h for the following 3 days, and finally the changes were noted after 72 h of period. The highest concentration which did not show cellular toxicity was considered as maximum nontoxic concentration of the compound. To more, the cytotoxicity concentration was confirmed by MTT (3-(4, 5-dimethylthiazol-2-YL)-2, 5-diphenyltetrazolium bromide) assay. In this assay, after 72 h of incubation of 96 well plate, 20 µL of (MTT) solution (5 mg/mL) was mixed in all the wells with the plate incubated at 37 °C with 5% CO_2 for 4 h. After 4 h of incubation, the medium in the plate was carefully removed without disturbing the cell monolayer. Finally, a volume of 120 µL of DMSO was mixed to the wells to dissolve the formazan crystals and read at 510 nm and 650 nm. The formula utilized for measuring cell viability percentage is as follows: the percentage of cell viability = treated × 100%/untreated.

In vitro antioxidant activity (H_2O_2 and DPPH radical scavenging activity)

The antioxidant property was estimated by the H_2O_2 scavenging assay. The synthesized compound HHDIP at different concentrations from 100 to 1000 µg/mL prepared in ethanol was mixed to 0.6 mL of H_2O_2 solution. The absorbance of the mixture of reaction was read after 15 min of evolution at 230 nm. The blank solution possesses an H_2O_2 solution without any compound. H_2O_2 scavenging activity of synthesized compounds was calculated as

$$\text{Hydrogen peroxide scavenging}\,(\%) = \left(A_0 - A_1\right)/A_0 \times 100$$

where A_0 is the absorbance of the control and A_1 is the absorbance of the sample.

The antioxidant potential of the synthesized compound was analyzed based on the scavenging of free radicals using 1,1-diphenyl-2-picrylhydrazyl (DPPH) method. In this method, 0.1 mM (ethanolic DPPH) was prepared as well as added with the test solution of synthesized titular compound HHDIP at different concentrations ranging from 100 to 500 µg/mL. After that, it was incubated for 30 min. Its absorbance was evaluated at 517 nm using (Beckman spectrophotometer). The discolorations were estimated with accurate blank at 517 nm after 30-min incubation at 30 °C in the dark. Calculations were performed in triplicate. In this investigation, uses of standard drug are D-ascorbic acid, and DPPH was absorbed in 517 nm, and also concentration was decreased using the activity of antioxidant. The free-radical scavenging activity percentage of the HHDIP was measured using the following formula:

$$\text{Scavenging } \% = \frac{1 - A_{\text{sample}} - A_{\text{blank}}}{A_{\text{control}}} \times 100$$

Here, ethanol (3 mL) with the solution sample (0.1 mL) was utilized as the blank, and 3 ml of DPPH solution with EtOH (0.1 ml) was utilized as the negative control.

Molecular docking and ADMET properties

Human c-Met Kinase (PDB code: 3F66) in complex with quinoxaline inhibitor was chosen as a protein target for molecular docking studies. X-ray diffraction resolution of 3F66 was 1.4Å. The preparation of recovered protein was accomplished using the made protein wizard of Discovery studio 4.0 [30–32]. The HHDIP ligand was prepared by using Discovery studio 4.0 small molecule tools for further use in molecular docking studies. The ADMET properties and toxicity profile outcomes such as non-mutagen and non-carcinogen in natures were estimated by computational analysis. Primarily, all the internal ligand, water molecules, ions and metal elements were removed. The active site was predicted from the prepared protein by the current selection method in the protein 3F66 B-chain. The amino acid residues obtained in the active site of target proteins such as B: ILE1084 B: ALA1108 B: LUE1157 B: PRO1158 B: TYR1159 B: MET1160 B: LYS1161 B: MET1211 were utilized for the docking with HHDIP. The structure of the synthesized ligand HHDIP was drawn using ChemDraw12.0 software. The synthesized 2D compound structure was changed into mol format, and that was further converted into 3D structure by Accelrys Discovery Studio V.4.0. This ligand was purified and prepared by Discovery studio4.0 small molecule tools for further use in molecular docking studies. The properties of ADMET and toxicity contours such as non-mutagen and non-carcinogen in nature of the HHDIP were estimated by computational analysis.

Results and discussion

Chemistry

The innovative method for the newly synthesized protocol of HHDIP was prepared by a three-step reaction. (Step I) 10H-phenothiazine **1** by the reaction with 10-hexyl-10H-phenothiazine **2** with reagents such as n-bromohexane, K_2CO_3 and DMF solvents has refluxed at 120 °C for 24 h. K_2CO_3, was originated to be an efficient catalyst for this reaction. (Step II) 10-hexyl-10H-phenothiazine-3-carbaldehyde **3** was prepared by the reaction of $POCl_3$/DMF under N_2 atmosphere for 24 h. Here, the $POCl_3$/DMF was utilized as Vilsmeier reagent, which served as an effective formylating agent. (Step III) The final product (HHDIP) was prepared by the reaction of benzil **4**, hexan-1-amine **5** with NH_4OAC withCH_3COOH reflux at 70–90 °C for 3 h. The complete reaction is exhibited in Scheme 1 which obtained a final product with a significantly high yield of 95% which is given in Table 1. The significance of this final product HHDIP has multidonor and multiacceptor

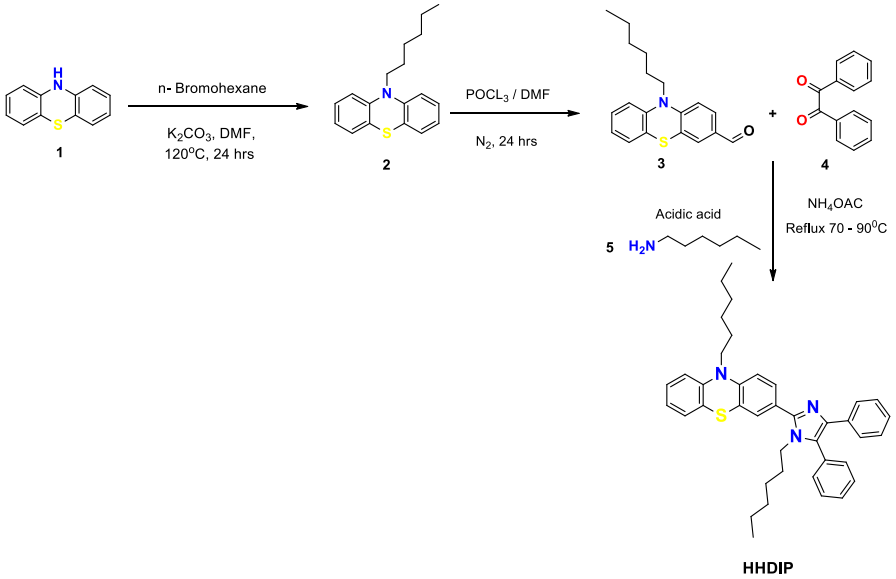

Scheme 1 General scheme of the synthesis of compound (HHDIP)

groups that are located in imidazole and phenothiazine ring. It also revealed better anticancer activity in our research. Some types of biologically important compounds of imidazoles are represented in Fig. 1.

Geometric structure

Thirty-nine optimized step numbers are obtained in the potential energy curve analysis method. The minimum energy value of −2074.04 a.u. is exhibited in Fig. 2. The optimized structure of HHDIP is shown in Fig. 3. It has C_1 point group symmetry. The optimized parameter of geometry like bond angles as well as bond lengths is computed by the DFT method using 6-311G++ (d,p) basis set, which is given in Tables 2 and 3 [33–35]. The optimized structure showed a mild alteration in the calculated C–C bond distances in the phenyl ring such as C1–C2, C9–C10 and C4–C12, respectively, for their values of 1.410, 1.407 and 1.393 A^0. The excellent outcomes of various bond lengths, respectively, C35–C36, C16–C21, and C32–C34 bonds are more significantly greater to thereof another C–C bond. This was owing to the producing electron in the substituents amino group, which is placed in the hydrogen atoms. Also, the benzene ring symmetry was distorted because of the replacement of hydrogen atoms. For example, C22–C19–C23 and C27–C20–C28 bond angles computed at 118.5 and 118.5^0 were incredibly matching the reported values [36]. Similarly; C2–C9–C10, C4–C12–C10, C1–C4–C12, C5–C6–C13, C9–C10–C11 and C17–C19–C23 were somewhat superior to 120^0 as shown in Table 3.

is of 10-hexyl-3-(1-hexyl-4,5-diphenyl-1H-imidazol-2-yl)-10H-phenothiazine HHDIP

-10H-phenothiazine-3-carbaldehyde (Benzil) **4**

HHDIP

Product	Yield (%)
HHDIP	95

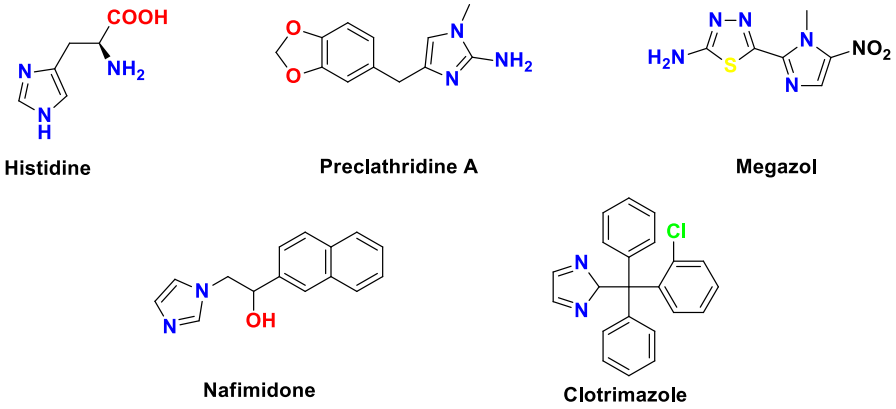

Fig. 1 Biologically important compounds of imidazole

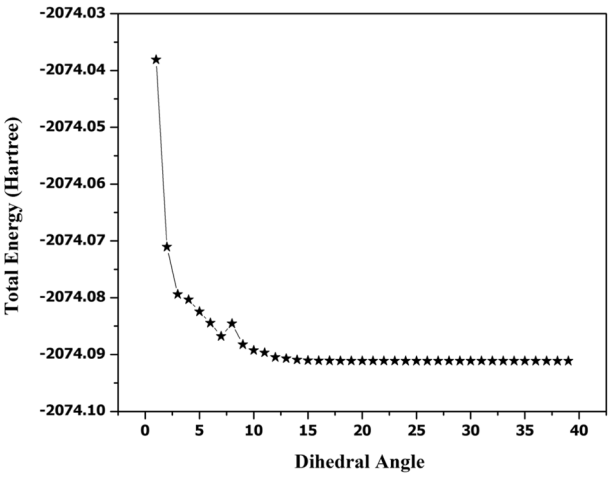

Fig. 2 Potential energy curve using DFT/B3LYP method with 6-311 ++G (d,p) basis set for HHDIP

Vibrational analysis

In this study HHDIP is detected 86 atoms, belongs to the C_1 point group, and has 252 normal modes of vibration. The final assignments of FTIR as well as FT-Raman spectra were done by experimental and theoretical analysis. Further, the harmonic vibrational frequencies are calculated for the HHDIP compound by DFT/B3LYP level with 6-311G++ (d,p) basis of theory. The percentage of (PED) potential energy distribution values for the experimental and calculated frequencies of the target compound are reported in Table S1 (Supplementary Material). In FTIR and FT-Raman spectra, to create an assessment between the experimental observation and theoretically calculated correlation coefficient, graphs are presented in Figs. S1 and S2 (Supplementary Material). Observed from the

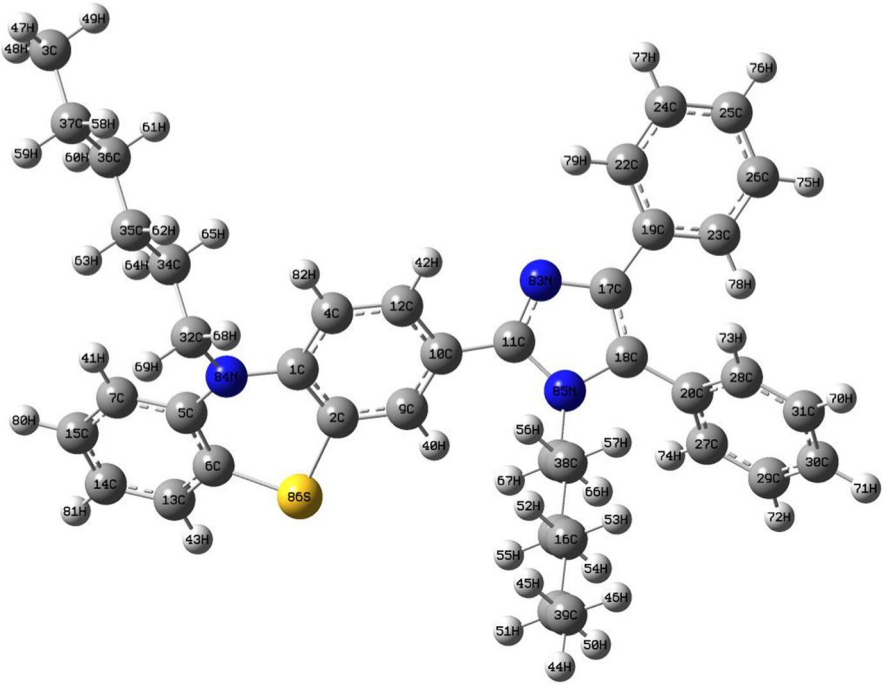

Fig. 3 Optimized theoretical geometric structure of 10-hexyl-3-(1-hexyl-4,5-diphenyl-1H-imidazol-2-yl)-10H-phenothiazine (HHDIP)

correlation graphs, the FTIR correlation coefficient (CC) R^2 is 0.99809 and the FT-Raman (CC) R^2 value is 0.99999 at B3LYP/6-311G++ (d,p) level. The experimental and calculated FTIR, as well as FT-Raman spectrum images, is demonstrated in Figs. 4 and 5; the computed frequencies are in good agreement with the FTIR as well as FT-Raman experimental values. The Gauss Sum 3.0 program has been used to obtain calculated FTIR and FT-Raman spectrum images [37]. For complete HHDIP, vibrational assignments are important under four heads: (i) aromatic C–H vibration, (ii) aromatic (C=C) stretching, (iii) C–N stretching vibration and (iv) C–S vibration.

CH vibration

The aromatic structures of C–H stretching vibrations are revealed in the region at 3306–3342 cm^{-1} [38] and 3150–2900 cm^{-1}, which is the characteristic region utilized for the prediction of C–H stretching vibration bands that are not affected [39]. In the title compound, FTIR and FT-Raman, the bands discovered at 3290, 3325, 2974, 2881 cm^{-1}, and 3239, 3118, 3036 cm^{-1}, respectively, are assigned to the C–H stretching vibrations. Different bending vibrations such as β HCC were observed at the region of 1563–125 cm^{-1}, and β HCH was observed in the range at

Table 2 Calculated bonds length (Å) of the molecule with DFT theory employing 6-311G++(d,p) basis set

Atom no.	B3LYP/6-311G++ (d,p)	Atom no.	B3LYP/6-311G++ (d,p)
C1–C2	**1.410**	C21–C38	1.539
C1–C4	1.413	C21–H54	1.101
C1–N84	1.419	C21–H55	1.101
C2–C9	1.393	C22–C24	1.396
C2–S86	1.835	C22–H79	1.084
C3–C37	1.537	C23–C26	1.398
C3–H47	1.096	C23–H78	1.083
C3–H48	1.097	C24–C25	1.401
C3–H49	1.097	C24–H77	1.086
C4–C12	**1.393**	C25–C26	1.399
C4–H82	1.08	C25–H76	1.086
C5–C6	1.411	C26–H75	1.086
C5–C7	1.412	C27–C29	1.399
C5–N84	1.423	C27–H74	1.086
C6–C13	1.395	C28–C31	1.398
C6–S86	1.836	C28–H73	1.085
C7–C15	1.398	C29–C30	1.400
C7–H41	1.08	C29–H72	1.086
C8–C16	1.54	C30–C3\)	1.400
C8–C39	1.537	C30–H71	1.085
C8–H50	1.100	R(31–70)	1.085
C8–H51	1.100	**C32–C34**	**1.546**
C9–C10	**1.407**	C32–H68	1.096
C9–H40	1.084	C32–H69	1.096
C10–C11	1.467	C32–N84	1.479
C10–C12	1.405	C33–C38	1.539
C11–N83	1.334	C33–H66	1.093
C11–N85	1.394	C33–H67	1.09
C12–H4)	1.084	C33–N85	1.476
C13–C14	1.399	C34–C35	1.540
C13–H43	1.085	C34–H64	1.097
C14–C15	1.396	C34–H65	1.097
C14–H81	1.084	**C35–C36**	**1.539**
C15–H80	1.085	C35–H62	1.101
C16–C21	**1.540**	C35–H63	1.101
C16–H52	1.101	C36–C37	1.540
C16–N53	1.101	C36–H60	1.101
C17–C18	1.394	C36–H61	1.101
C17–C19	1.471	C37–H58	1.100
C17–N83	1.394	C37–H59	1.100
C18–C20	1.476	C38–H56	1.098
C18–N85	1.407	C38–H57	1.098

Table 2 (continued)

Atom no.	B3LYP/6-311G++ (d,p)	Atom no.	B3LYP/6-311G++ (d,p)
C19–C22	1.410	C39–H44	1.096
C19–C23	1.409	C39–H45	1.097
C20–C27	1.410	C39–H46	1.097
C20–C28	1.410		

1461–1342 cm^{-1}[40]. In our present study, the experimental FTIR bending β HCC vibrations are discovered at 1328 and 1030 cm^{-1} with PED contribution values of 22 and 32%. In FT-Raman, it was obtained experimentally at 1509 cm^{-1} with a PED contribution at 21%. Furthermore, in FT-Raman, the bending vibration of β CNC is observed theoretically at 988 cm^{-1}, and experimentally, it is well matched in 984 cm^{-1} (mode number 101) with a PED contribution of 17%.

Moreover, some HCN, CCN and CCC bending vibrations are obtained in the HHDIP compound and HCCH, HCCC, CCCC and HCCH torsion vibrations were obtained in HHDIP, which have a great deal with the literature [41–43].

Phenyl ring vibrations

The aromatic C=C stretching phenyl group vibrations are predicted in the range from 1650–1200 cm^{-1} [44]. Hence, in the FTIR strong vibrational frequency band at 1654 cm^{-1} is assigned to C=C stretching vibrations experimentally, which matches well with the calculated vibrational band at 1662 cm^{-1}, respectively; the medium intensity bands experimentally at 1087 and 1045 cm^{-1} with the mode numbers of 123 and 115 are also reasoned to C=C stretching and coincide well with the computed frequency values at 1085 cm^{-1} and 1051 cm^{-1} with a 62% and 25% of PED contribution. However, in FT-Raman studies, the strong vibrational frequency bands were recorded experimentally at 1667 and 1601 cm^{-1}, which is perfectly matched with calculated vibrational bands at 1666 and 1604 cm^{-1} with the mode numbers of 208 and 202.

C–N and C–S vibrations

The prediction of C–N stretching frequency is a very challenging task because of the C–N Composite region falls on the vibrational spectrum; specifically, mixing of the various bands is the promising assignment of C–N stretching region at 1386–1266 cm^{-1} for the aromatic compound [45, 46]. In this present analysis, the C–N stretching vibrations of HHDIP are found at 1274 cm^{-1} in FTIR and 1272 cm^{-1} in the FT-Raman spectrum, and also they have presented PED contribution value of 13 and 10% with the mode numbers of 145 and 144. The carbon–sulfur (C–S) stretching vibration shows in the region at 570–380 cm^{-1} [47]. In the present studies,

Table 3 Calculated bond angles (°) of the molecule with DFT theory employing 6-311G++(d,p) basis set

Structural parameters	B3LYP/6-311G++(d,p)	Structural parameters	B3LYP/6-311G++(d,p)
C2–C1–C4	116.6	C18–C20–C27	121.0
C2–C1–N84	122.1	C18–C20–C28	120.5
C1–C2–C9	121.8	C18–N85–C33	124.2
C1–C2–S86	120.4	**C22–C19–C23**	**118.5**
C4–C1–N84	121.3	C19–C22–C24	120.8
C1–C4–C12	**121.7**	C19–C22–H79	118.3
C1–C4–H82	120.2	C19–C23–C26	120.7
C1–N84–C5	122.6	C19–C23–H78	120.0
C1–N84–C32	118.4	**C27–C20–C28**	**118.5**
C9–C2–S86	117.7	C20–C27–C29	120.7
C2–C9–C10	**121.2**	C20–C27–H74	119.2
C2–C9–H40	118.4	C20–C28–C31	120.7
C2–S86–C6	98.50	C20–C28–H73	119.1
C37–C3–H47	111.4	C38–C21–H54	109.4
C37–C3–H48	111.1	C38–C21–H55	109.4
C37–C3–C49	111.1	C21–C38–C33	112.0
C3–C37–C36	113.0	C21–C38–H56	109.9
C3–C37–H58	109.5	C21–C38–H57	109.9
C3–C37–H59	109.5	H54–C21–H55	106.4
H47–C3–H48	107.8	C24–C22–C79	120.9
H47–C3–H49	107.8	C22–C24–C25	120.4
H48–C3–H49	107.6	C22–C24–H7)	119.6
C12–C4–H82	118.1	C26–C23–H78	119.3
C4–C12–C10	**121.3**	C23–C26–C25	120.5
C4–C12–H42	119.9	C23–C26–H75	119.5
C6–C5–C7	117.0	C25–C24–H77	120.0
C6–C5–N84	121.9	C24–C25–C26	119.3
C5–C6–C13	**121.6**	C24–C25–H76	120.4
C5–C6–S86	120.4	C26–C25–H76	120.3
C7–C5–N84	121.1	C25–C26–H75	120.0
C5–C7–C15	121.4	C29–C27–H74	120.0
C5–C7–H41	120.2	C27–C29–C30	120.2
C5–N84–C32	118.4	C27–C29–H72	119.7
C13–C6–S86	117.8	C31–C28–H73	120.2
C6–C13–C14	120.6	C28–C31–C30	120.3
C6–C13–H43	119.0	C28–C31–H70	119.7
C15–C7–H41	118.4	C30–C29–H72	120.1
C7–C15–C14	120.6	C29–C30–C31	119.7
C7–C15–H80	119.0	C29–C30–H71	120.2
C16–C8–C39	113.1	C31–C30–H71	120.2

Table 3 (continued)

Structural parameters	B3LYP/6-311G++ (d,p)	Structural parameters	B3LYP/6-311G++ (d,p)
C16–C8–H50	109.2	C30–C31–H70	120.1
C16–C8–H51	109.1	C34–C32–H68	109.4
C8–C16–C21	113.3	C34–C32–H69	109.4
C8–C16–H52	109.2	C34–C32–N84	116.9
C8–C16–H53	109.2	C32–C34–C35	111.4
C39–C8–H50	109.5	C32–C34–H64	110.2
C39–C8–H51	109.5	C32–C34–H65	110.2
C8–C39–H44	111.4	H68–C32–H69	106.4
C8–C39–H45	111.0	H68–C32–N84	107.2
C8–C39–H46	111.1	H69–C32–N84	107.1
C50–H8–C51	106.2	C38–C33–H66	110.2
C10–C9–H40	120.4	C38–C33–H67	109.8
C9–C10–C11	**123.4**	C38–C33–N85	112.6
C9–C10–C12	117.4	C33–C38–H56	108.9
C11–C10–C12	119.1	C33–C38–H57	109.1
C10–C11–N83	123.1	H66–C33–H67	107.6
C10–C11–N85	126.3	H66–C33–N85	108.0
C10–C12–H42	118.8	H67–C33–N85	108.4
N83–C11–N85	110.5	C35–C34–H64	109.6
C11–N83–C17	107.2	C35–C34–H65	109.6
C11–N85–C18	107.0	C34–C35–C36	113.2
C11–N85–C33	126.5	C34–C35–H62	109.4
C14–C13–H43	120.4	C34–C35–H63	109.4
C13–C14–C15	118.8	H64–C34–H65	105.6
C13–C14–H81	120.2	C36–C35–H62	109.2
C15–C14–H81	120.9	C36–C35–H63	109.2
C14–C15–H80	120.3	C35–C36–C37	113.4
C21–C16–H52	109.3	C35–C36–H60	109.3
C21–C16–H53	109.3	C35–C36–H61	109.3
C16–C21–C38	113.0	H62–C35–H63	106.1
C16–C21–H54	109.2	C37–C36–H60	109.2
C16–C21–H55	109.2	C37–C36–H61	109.2
H52–C16–H53	106.3	C36–C37–H58	109.2
C18–C17–C19	131.1	C36–C37–H59	109.2
C18–C17–N83	109.4	H60–C36–H61	106.2
C17–C18–C20	132.0	H58–C37–H59	106.2
C17–C18–N85	105.9	H56–C38–H57	107.0
C19–C17–N83	119.5	H44–C39–H45	107.8
C17–C19–C22	118.7	H44–C39–H46	107.8
C17–C19–C23	**123.0**	H45–C39–H46	107.6
C20–C18–N85	122.1		

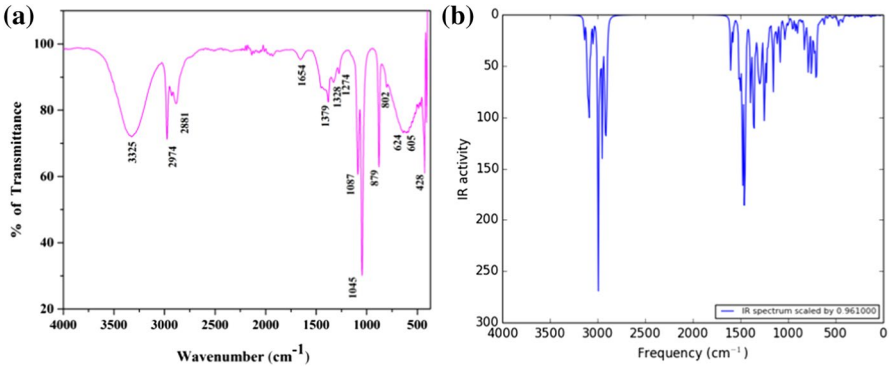

Fig. 4 Experimental FTIR spectrum of (HHDIP) (**a**) and theoretical FTIR spectrum of (HHDIP) (**b**) at DFT/B3LYP/6-311G++ (d,p)

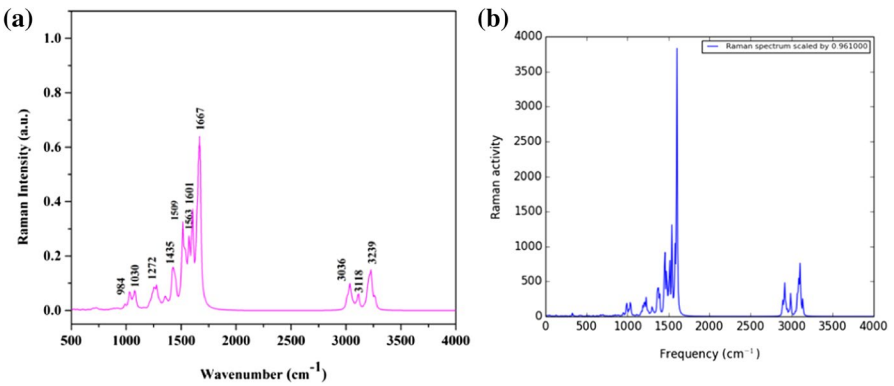

Fig. 5 Experimental FT-Raman spectrum of (HHDIP) (**a**) and theoretical FT-Raman spectrum of (HHDIP) (**b**) at DFT/B3LYP/6-311G++ (d,p)

the calculated wave numbers show region at 452 cm^{-1} (mode no. 51) with 11% of PED contribution which is assigned as C–S stretching vibration.

The experimental C–S stretching bands region was determined at 428 cm^{-1} for HHDIP, respectively, which is in good agreement with the computed value.

NLO properties

The improvements in NLO material properties gained an enormous interest in the past few periods. These materials have revealed various device uses such as an optical switches, electronics device, telecommunications, optical interconnections and signal processing [48–51]. These are very important in areas such as linear polarizability (α), total molecular dipole moment (μ) and first-order hyperpolarizability (β), which are calculated by B3LYP/6-311G++ (d,p) basis set from Gaussian 09W. The calculation of the magnitude of total molecular dipole moment (μ), linear

polarizability (α), the anisotropy of the polarizability ($\Delta\alpha$) and first-order hyperpolarizability (β) from complete equations is given below [52, 53]:

$$\mu_{\text{total}} = \mu_0 + \alpha_{ij}E_j + \beta_{ijk}E_jE_k + \tag{1}$$

$$\alpha_{\text{tot}} = \frac{1}{3}\left(\alpha_{xx} + \alpha_{yy} + \alpha_{zz}\right) \tag{2}$$

$$\Delta\alpha = 2^{-1/2}\left[\left(\alpha_{xx} - \alpha_{yy}\right)^2 + \left(\alpha_{yy} - \alpha_{zz}\right)^2 + \left(\alpha_{zz} - \alpha_{xx}\right)^2 + 6\alpha_{xz}^2\right]^{1/2}. \tag{3}$$

$$\beta_{\text{tot}} = \left(\beta_x^2 + \beta_y^2 + \beta_z^2\right)^{1/2} \tag{4}$$

$$\beta_{\text{tot}} = \left[\left(\beta_{xxx} + \beta_{xyy} + \beta_{xzz}\right)^2 + \left(\beta_{yyy} + \beta_{yzz} + \beta_{xxy}\right)^2 + \left(\beta_{zzz} + \beta_{xxz} + \beta_{yyz}\right)^2\right]^{1/2} \tag{5}$$

The title molecule NLO properties was calculated with its results of the total molecular dipole moment value of ($\mu = 3.3231$ Debye) and mean the first hyperpolarizability value of ($\beta_{\text{tot}} = 6.49 \times 10^{-30}$ esu), which are specified in Table 4, and its total dipole moment of the molecule is approximately two times higher than that of urea and the first hyperpolarizability is 15 times higher than that of

Table 4 Calculated electronic dipole moment (μ), linear polarizability (α), anisotropy of polarizability ($\Delta\alpha$), first-order hyperpolarizability (β) values for HHDIP by DFT/B3LYP/6-311G++ (d,p) level of theory

Parameter	Value	Parameter	a.u.	esu(x10^{-24})	Parameter	a.u.	esu(x10^{-33})
μ_x	1.1123	α_{xx}	221.255	32.789	β_{xxx}	−25.376	−219.230
μ_y	2.380	α_{xy}	16.774	2.486	β_{xxy}	−31.934	−275.896
μ_z	2.035	α_{yy}	267.953	39.710	β_{xyy}	11.224	96.967
μ	3.3231	α_{xz}	3.225	3.703	β_{yyy}	25.075	216.630
		α_{yz}	9.024	1.337	β_{xxz}	−13.118	−113.330
		α_{zz}	260.589	38.619	β_{xyz}	−11.820	−102.116
		α_{tot}	249.929	37.039	β_{yyz}	11.139	96.493
		$\Delta\alpha$	480.558	71.219	β_{xzz}	−19.934	−172.2166
					β_{yzz}	−37.454	−323.5757
					β_{zzz}	−0.433	−3.740
					β_{tot}	750.589	6484.564
					$\beta_{\text{tot}}^{-31} = 64.84 \times 10$ esu		

The values of the first-order hyperpolarizability (β) tensors of Gaussian09W output are reported in atomic units (a.u)

The calculated (DFT) values were converted into electrostatic units (For α: 1a.u. = 0.1482×10^{-24} esu; for β: 1a.u. = 8.6393×10^{-33} esu)

urea (μ and β values of urea are $\mu = 1.3732$ Debye and $\beta_{tot} = 0.3728 \times 10^{-30}$esu, 6-311G++(d,p), respectively [54]. Hence, this molecule has a higher dipole moment and hyperpolarizability value than urea which shows that the molecule has a large applicant for nonlinear optics (NLO) material.

Thermodynamic study

The thermodynamics parameter of HHDIP is computed to obtain authentic relations between structural, energetic and reactivity characteristics of the molecules. Selective information on the stable (dipole moment) of a molecule permits us to find out the molecule's confirmation. The calculated thermodynamic properties by using a basic set of B3LYP/6-311G ++ (d,p) as well as their outcomes values are given in Table 5. The frequency calculations are utilized to find out the Gibbs free energies, enthalpy, entropy and the heat capacity for a molecular system. Higher values of Gibbs free energies signify more stable molecules [55]. The enthalpy, entropy, zero-point vibrational energy (ZPVE) and heat capacity values are found at any temperature and are helpful in evaluating the direction of chemical reactions. The dipole moment (Debye) parameter value is completed by using this study. The valuable outcomes of the synthesized HHDIP free energy, entropy, enthalpy and ZPVE are utilized.

Mulliken's population analysis

This study plays a vital role of application in quantum chemical approach to the molecular system by atomic charge effect, molecular polarizability, dipole moment, electronic structure, and other molecular properties that are affected by the atomic charge. Mulliken atomic charge distribution for the HHDIP is presented in Fig. S3 (Supplementary Material), and Mulliken plot of charge distribution for the title compound is exhibited in Fig. 6. From Fig. S3 (Supplementary Material) and Fig. 6, it is distinctly found that the charge of nitrogen atoms N83, N84, and N85 of the HHDIP compound is highly negative and the corresponding protonated hydrogen H79 atom possesses higher positive charge compared to other hydrogen atoms. The C5 carbon atom is shown highly positive charge which is located phenothiazine group and thereof nearby located phenothiazine, as well as imidazole rings, are containing

Table 5 Theoretically computed thermodynamic parameters of HHDIP by B3LYP/6-311G++(d,p) basis set

Thermodynamic parameters	HHDIP
Total energy (Hartrees)	−2075.0912
Enthalpy (Hartrees)	0.7816
Gibbs free energy (Hartrees)	0.6600
Zero-point vibrational energy (Kcal mol^{-1})	464.6521
Heat capacity (cal mol^{-1} K^{-1})	153.1701
Entropy (cal mol^{-1} K^{-1})	255.6542
Dipole moment (Debye)	3.3231

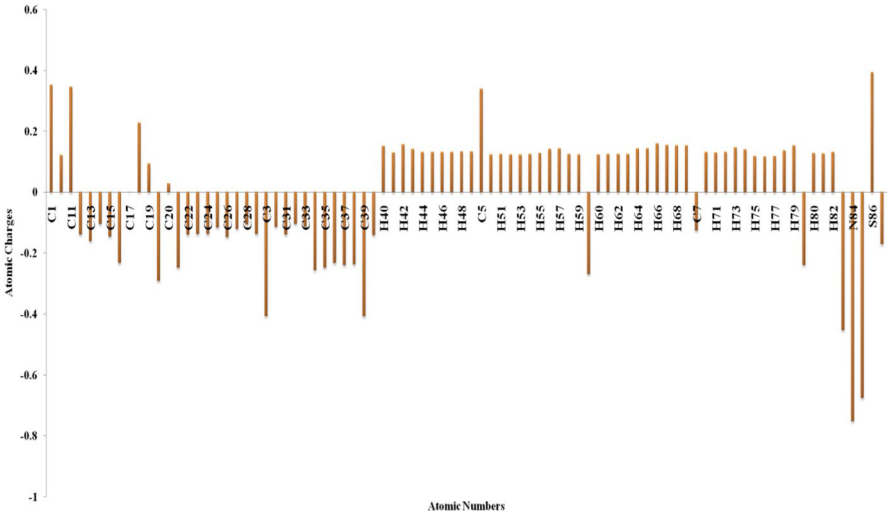

Fig. 6 Mulliken plot of atomic charge distribution for HHDIP

eight carbon atoms namely C3, C39, C13, C16, C19, C21, C34, and C35 have a higher negative influence. In this investigation, aromatic rings have negative values on C15, C37, C22, C23, C24, C26, C27, C25 and C40 atoms which leads to reallocation of the electron density. As an outcome of these strong negative charges, C1 and C11 accommodate large positive charge and are higher acidic.

Moreover, it is also noticed that the sulfur atom S86 attains maximum positive charge owing to its bonding with electronegative nitrogen atom N84. Table S2 (Supplementary Material) gives the total atomic charges (ground state) of HHDIP which are found from DFT/B3LYP/6-311++G (d,p) level.

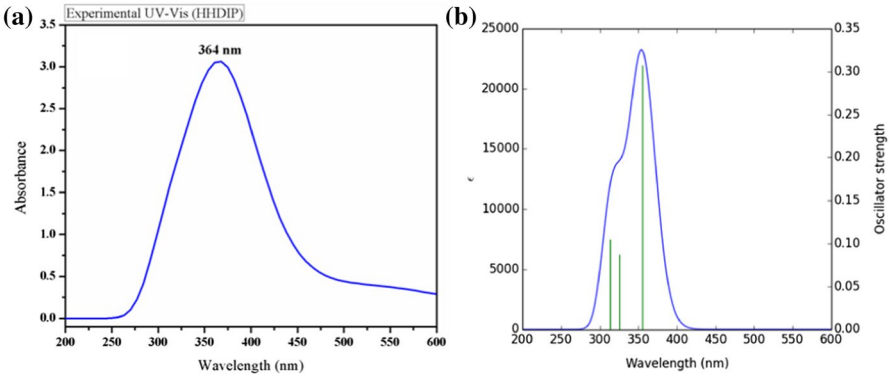

Fig. 7 UV–Vis spectra of HHDIP experimental (**a**) and theoretical (**b**) (GAS phase))

UV–Vis spectral analysis

The experimental and computational UV–Vis comparability spectrum investigation HHDIP is represented in Fig. 7, and its absorption maximum (λmax) is calculated by TD-DFT/B3LYP method with a 6-311++G (d,p) basis set. The stimulated molecular orbital geometry indicates a visible absorption maximum of the HHDIP is matched to the (HOMO–LUMO) electronic transition in (gas phase).

The electronic transition among the transformation from (HOMO–LUMO) transformation can be observed by using UV–Vis spectra absorption values of 364 nm and band gap 3.3086 (eV) (Experimental). The experimental energy value of band gap has estimated utilizing the formula, $E = hc/\lambda$. Here, h and c are constant; λ is the cutoff wavelength [56, 57]. The title molecule theoretically observed value of 355.70 nm (gas phase), oscillator strength value of ($f = 0.3073$), and band gap energy value of 3.4856(eV), which are presented in Table 6; the experimental and theoretical UV data are in good agreement with each other. The calculated UV–Vis spectrum is plotted with the Gauss Sum 3.0 program [17]. The computed absorption spectrum reveals that the highest range of UV–Vis absorption wavelength complies from the HOMO–LUMO electronic transition with (80%) contribution [58].

Frontier molecular orbitals (FMOs) analysis

Analysis of FMOs is utilized to confirm the molecular interactions, which has huge significance in recent biochemistry and molecular biology [59]. It provides evidence about the properties of ligand molecules as well as their interactions with the biological receptor. Analysis of HOMO–LUMO outcome of HHDIP is revealed in Fig. 8. HOMO (highest occupied molecular orbital) and LUMO (lowest unoccupied molecular orbital) orbitals compute the electron–donor and electron–acceptor character, respectively. Table 7 gives the values of FMOs associated with molecular properties [60].

The computed lofty ionization potential value of HHDIP reveals the capacity to carry out a nucleophilic attack. The band gap energy is an important for the stability of structures [61, 62]. Energy of HOMO–LUMO is associated with the electronic affinity as well as ionization potential. The DFT outcome of HOMO–LUMO energies, the energy gap (ΔE), the ionization potential (I), the electron affinity (A), the absolute electronegativity (χ), the absolute hardness (η), electrophilicity index (ω) and softness (S) for the HHDIP molecule energies are computed. The title molecule (HOMO)–(LUMO) energy gap values are obtained value of (−0.7992 eV) and (−4.8195 eV) which are also given lower softness value of 2.2099. The softness value helps in knowing the toxicity of several pollutants in terms of their reactivity and site selectivity. Measured band gap value (4.0203 eV) signifies that the HHDIP compound has a stable structure. The gas phase calculated using the B3LYP/6-311G++ (d,p) method provides outcomes as HHDIP possessed 157 occupied and 320 unoccupied molecular orbitals. Besides, the title compound (see Table 7)

Table 6 Theoretical and experimental electronic absorption spectra values of using TD-DFT/6-311G++ (d,p) method and their assignments

Molecule	Experimental λ_{max}(nm)	Band gap (eV)	Theoretical λ_{max}(n)	Band gap (eV)	Oscillator strength (f)	Assignment
HHDIP	364	3.3086	355.70	3.4856	0.3073	HOMO → LUMO (80%)

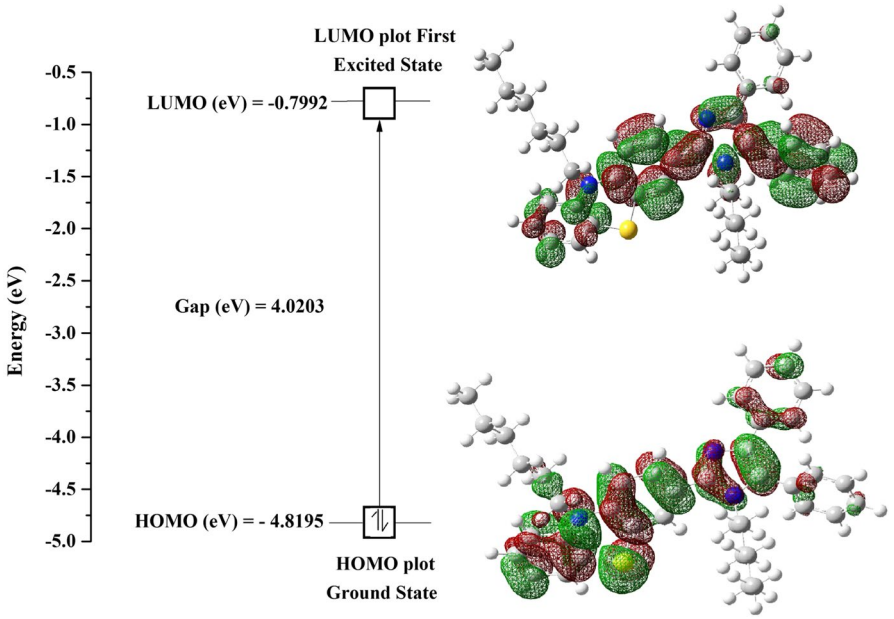

Fig. 8 Atomic orbital HOMO–LUMO composition of the frontier molecule orbital for HHDIP

Table 7 Calculated quantum chemical parameters HOMO–LUMO results of HHDIP

Quantum parameters (eV)	HHDIP (HOMO–LUMO)
E_{HOMO}	−4.8195
E_{LUMO}	−0.7992
ΔE_{gap}	4.0203
$I=-E_{\mathrm{HOMO}}$	4.8195
$A=-E_{\mathrm{LUMO}}$	0.7992
$\chi=\frac{I+A}{2}$	5.2191
$\mu=-(I+A)/2$	−5.2191
$\eta=I-A)/2$	4.4199
$S=\frac{1}{2\eta}$	2.2099
$\omega=\frac{\mu^2}{2\eta}$	3.0815

HOMO–LUMO has a high electrophilicity index value of 3.0815 and hence it is biologically active [63].

In HOMO–LUMO analysis, red color is represented as a positive phase and green color is represented as a negative phase. It is evident from the figure that the HOMO levels diffuse mainly over phenothiazine and partially slightly on the imidazole group. LUMO levels are diffused mostly over imidazole and partially presented on

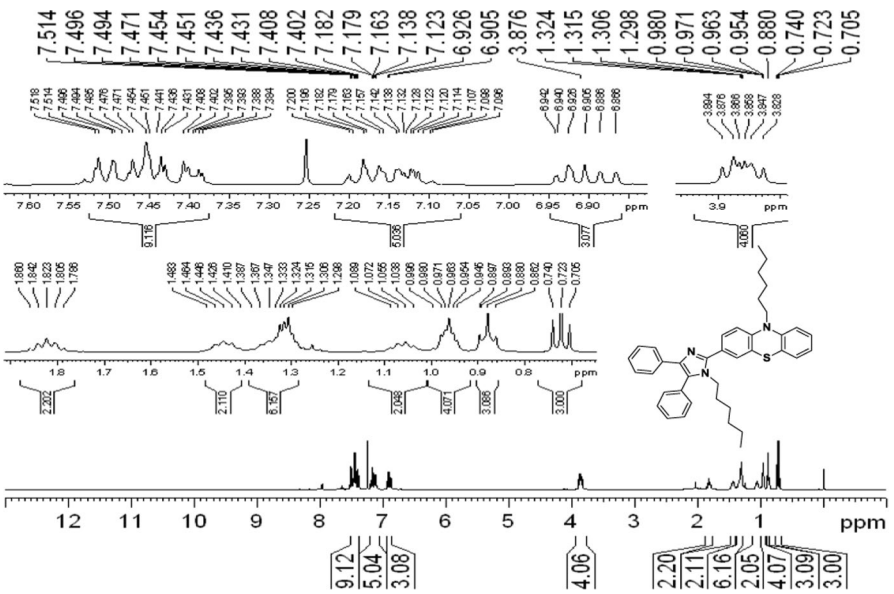

Fig. 9 Experimental ^{1}H spectrum of the title compound

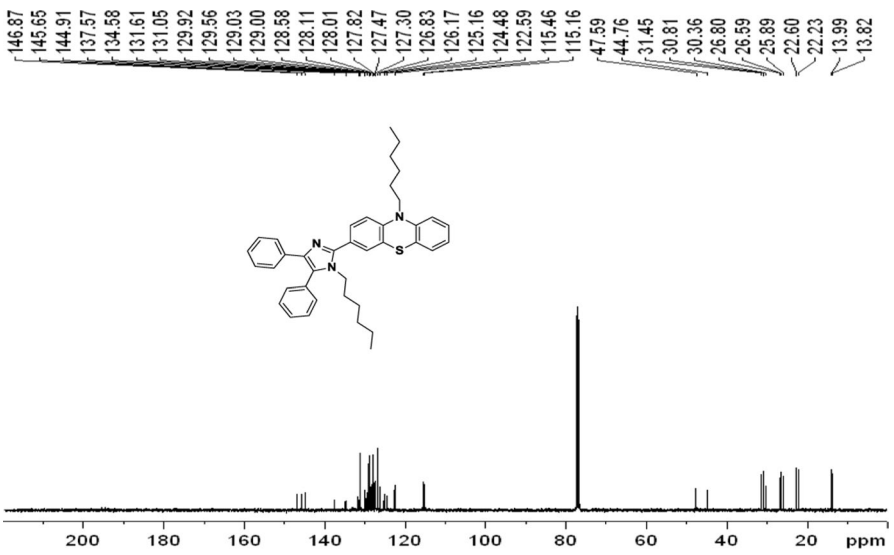

Fig. 10 Experimental ^{13}C spectrum of the title compound

the phenothiazine group [64]. The lower softness and higher hardness values signify molecule stability. The electrophilicity indexes as well as lower chemical potential values have exhibited the potential bioactive molecules [65].

^{1}H and ^{13}C NMR spectral studies

The NMR assists as a grand resource in deciding the structure of an organic compound by disclosing the hydrogen and carbon skeleton. To furnish a specific assignment and investigation ^{1}H as well as ^{13}C NMR spectra, theoretical chemical shift value of calculations in the HHDIP was done by gauge-independent atomic orbital (GIAO) manner at B3LYP/6-311++G (d,p) level with vacuum method. The ^{1}HNMR and ^{13}C NMR spectral studies of HHDIP showed peaks at different chemical shift values as given in Figs. 9 and 10. Theoretical and experimental chemical shift values are specified in Table S3 and S4 (Supplementary Material). The little difference observed among DFT and experimental spectra values is owing to the solvent used. The ^{13}C NMR chemical shifts, absolute shielding tetramethylsilane (TMS) values are 192.8847 and 31.8927 for ^{1}H NMR spectra. In this investigation, the title compound ^{1}HNMR spectrum chemical shifts are interpreted to conform to the promising different effects which act on the shielding constants of protons. Aromatic protons are seemed to be the downfield signals at d values of 6.880, 6.940, 7.090 and 7.200 for protons H43, H81, H41 and H75 which give multiplet (Ar–H) signals, which are located in phenothiazine group. Protons H76 and H77 give multiplet (Ar–H) signals, which are located in the benzil ring. The upfield protons are seemed to be from 1 to −5 (ppm), respectively. The methyl protons signal was presented at δ 0.740 (ppm) for proton H48 which gives a triplet. Furthermore, the methylene proton signal was shown at δ 0.890, 0.990, 1.030, 1.060, 1.080, 1.290, 1.330, 1.360, 1.380, 1.420, 1.440, 1.460, 1.480, 1.880, 3.820 and 3.890 (ppm) for protons H45, H55, H57, H47, H46, H49, H50, H55, H57, H63, H60, H51, H64, H56, H68 and H66 giving multiplet, which are located in hexyl group. In this analysis, the ^{13}C-NMR spectrum of aromatic carbons provides signals with chemical shift values from 100 to 200 ppm [66, 67]. The HHDIP chemical shifts (experimental) ranges take place in the range of δ 115.160–131.050 ppm, and phenothiazine carbons C13 and C1 are detected in the downfield at δ 145.910 and 146.870 ppm owing to the presence of the phenothiazine group. Due to the more electronegative sulfur atoms in the ring, the carbon atoms chemical shifts ranges are shown in the heterocyclic rings, which are set to the downfield. Therefore, the chemical shift of imidazole carbon C18 is also detected at the downfield at δ 131.610 ppm. The C33 carbon atom at δ 47.590 ppm is highly shielded which is located in the hexyl group of aliphatic carbon. Furthermore, the chemical shifts of benzil ring carbon atoms C24, C28, C19 and C20 are assigned to 124.480, 125.160, 127.820 and 128.580 ppm.

The calculated chemical shifts are in good agreement with the experimental values. As it can be detected from the graph, the correlation coefficient (CC) R^2 values are ^{1}HNMR 0.999 and 0.996 for ^{13}C NMR spectra. The correlation between the calculated and experimental ^{1}H and ^{13}C chemical shifts of HHDIP is represented in Figs. 11 and 12.

Mass spectrum

The mass spectrum range of synthesized compound HHDIP with its molecular ion peak observed at *m*/*z* 586.60 is owing to the presence of (MH+), which coincides with

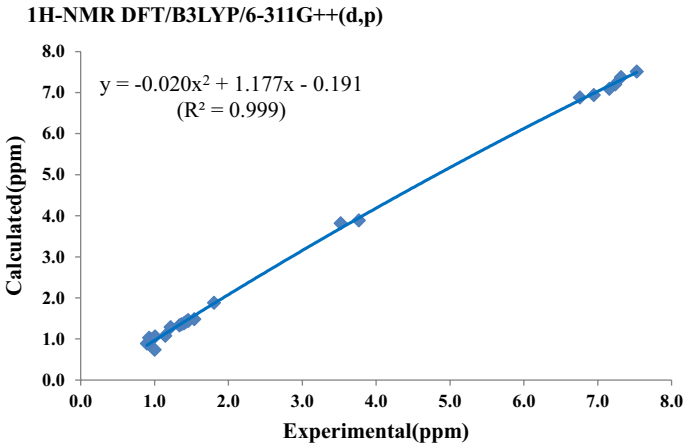

Fig. 11 Correlation graph between the experimental and simulated ^{1}H NMR chemical shift values of HHDIP

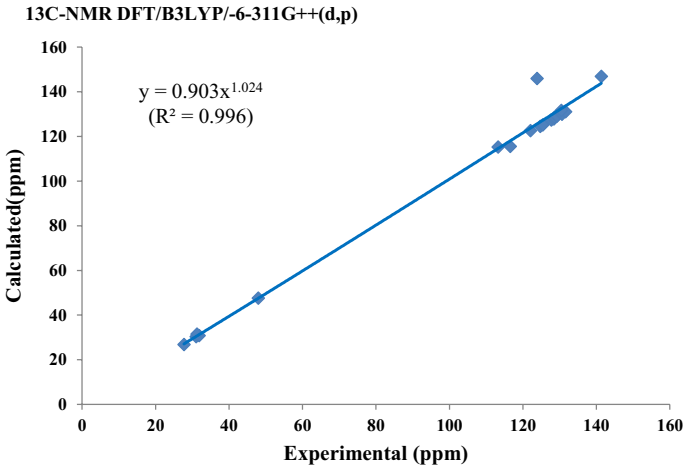

Fig. 12 Correlation graph between the experimental and simulated ^{13}C NMR chemical shift values of HHDIP

the molecular mass; their *m/z* scale ranges observed at 200–2000 are presented in Fig. S4 (Supplementary Material). The obtained molecular ion peaks in the spectra are in excellent agreement with the proposed molecular structures of the title compound. The spectrophotometers were run in positive scan mode.

Table 8 Anticancer activity of synthesized compound HHDIP measured by MTT assay and HepG2 liver cancer cell line

% of concentration (µg/ml)	% of cell viability HHDIP
15.75	78.7
31.25	74.4
62.5	**70.7**
125	60.2
250	**59.1**
Control	100

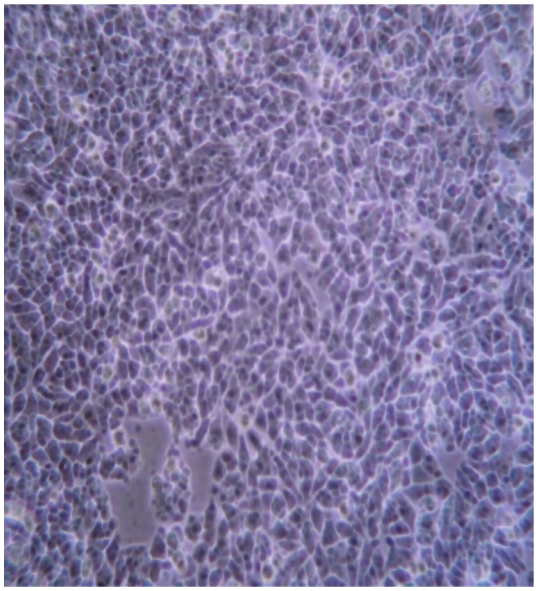

Fig. 13 HepG2 liver cancer cell lines—controls compound HHDIP—250 µg/mL

Biological section

In vitro anticancer activity

Most of the imidazole derivatives have been observed to be successful in vitro cytotoxic compounds against a human liver tumor cell line [68, 69]. In this investigation, new imidazole compound was synthesized for their anticancer activity. The title compound showed the anticancer activity at the lowest concentration of 62.5 µg/mL. This compound reduced the cell viability to 70.7%; the cell viability was much more decreased to 59.1% at 250 µg/mL. The HepG2 liver cancer cells were tested at concentrations from 15.75 µg/mL to 250 µg/mL given in Table 8. The (HepG2) liver cancer cell lines controls image is represented in Fig. 13. The title molecule showed potent anticancer activity against HepG2 cell line only at the higher concentration 250 µg/mL, which is represented in Fig. 14. The resultant (HepG2) graphical representation of HHDIP is given in Fig. 15.

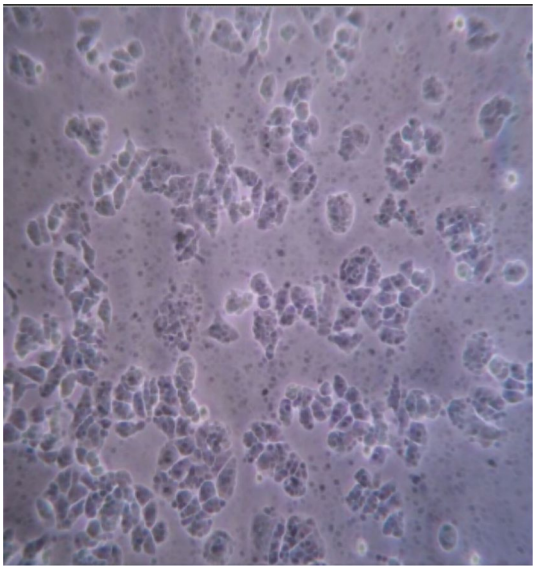

Fig. 14 HepG2 liver cancer cell lines image of HHDIP

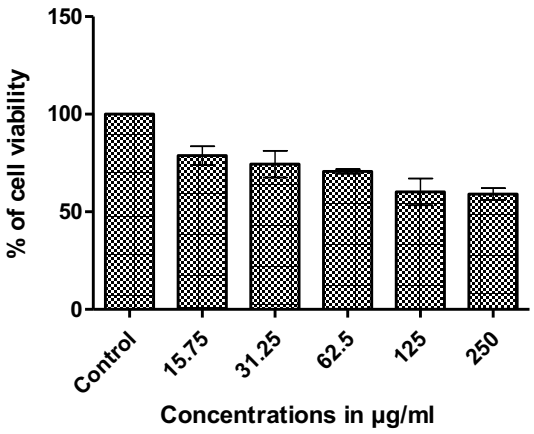

Fig. 15 Anticancer activities of synthesized compound HHDIP measured by MTT assay and HepG2 liver cancer cell line

In vitro antioxidant activity (H_2O_2 and DPPH radical scavenging activity)

The H_2O_2 scavenging assay was evaluated according to the method of some medications [70]. The outcomes of the antioxidant (H_2O_2) study have shown that using synthesized compound HHDIP was potentially a good source of hydroxyl radical scavenging activity. Hydroxyl radicals ($OH^{\cdot}$) are short-lived species having high affinity toward other molecules. The results of $OH^{\cdot}$ scavenging activity of synthesized compounds revealed that the title compound possessed strong antioxidant activity. The complete results of H_2O_2 in vitro antioxidant activities are shown in Table 9.

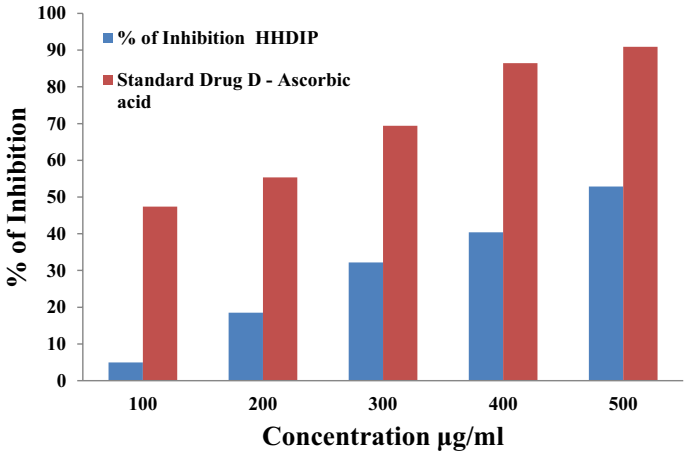

Fig. 16 *In vitro* DPPH radical scavenging activity of test compound 10-hexyl-3-(1-hexyl-4,5-diphenyl-1H-imidazol-2-yl)-10H-phenothiazine (HHDIP)

Table 9 Antioxidant activity of test compound 10-hexyl-3-(1-hexyl-4,5-diphenyl-1H-imidazol-2-yl)-10-pentyl-10H-phenothiazine (HHDIP) measured by H_2O_2 assay

Sample name	Control	Test (1 mg/mL)	H_2O_2 Scavenging (%)
HHDIP	3.8	1.28	66.31

Table 10 Antioxidant activity of test compound 10-hexyl-3-(1-hexyl-4,5-diphenyl-1H-imidazol-2-yl)-10-pentyl-10H-phenothiazine (HHDIP) measured by DPPH assay

Concentration (µg/ml)	% of inhibition HHDIP	Standard drug D-ascorbic acid
100	4.95604	47.363
200	18.5452	55.3158
300	32.1743	69.425
400	40.4077	86.45
500	52.8777	90.888

*Ascorbic acid was used as a standard at 100, 200, 300, 400 and 500 µg concentrations of compound/mL

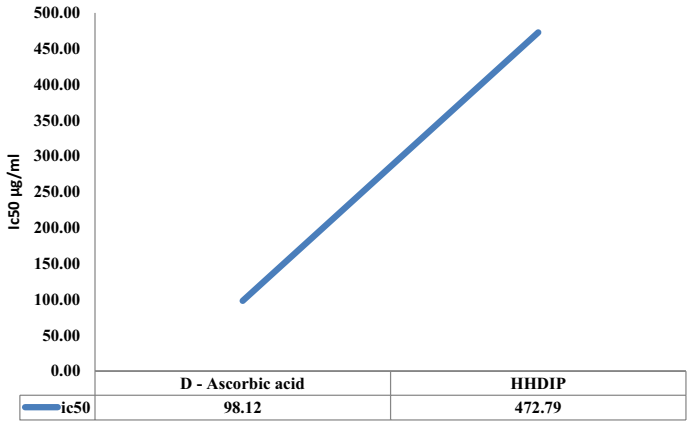

Fig. 17 Free-radical scavenging activities of the 10-hexyl-3-(1-hexyl-4,5-diphenyl-1H-imidazol-2-yl)-10H-phenothiazine (HHDIP) and vitamin C measured in DPPH assay

The synthesized title molecule was estimated for their potential to scavenge the free-radical formation, which was measured by the DPPH assay method [71, 72]. The HHDIP antioxidant activity is shown in Table 10. The D-ascorbic acid (vitamin C) was utilized as a standard antioxidant. The IC_{50} value for each compound was calculated, and it was found that the antioxidant tested compound HHDIP possesses IC_{50} value of 472.79 µg/mL (Fig. 17). When compared to the standards, HHDIP showed lowest free-radical scavenging activity at 52.8777% of inhibition, and D-ascorbic acid (Vitamin C) showed the activity of 90.888% of free-radical scavenging concentration at 500 µg/mL (Table 10). Finally, antioxidant test compound HHDIP has given satisfactory radical scavenging activity (Fig. 16).

In silico section

Molecular docking studies

In this investigation, the title compound showed significant in vitro anticancer activity. Hence, this compound was further studied by in silico molecular docking investigations against 3F66 (c-Met kinase; a hepatocyte growth factor) protein target. The receptor tyrosine kinases (RTKs) are a pharmaceutically attractive target that acted as a vital job in tumor formation and regulated the variety of signal-transduction pathways within a cell. New therapies are being developed according to the molecular profile of patients, especially based on the special involvement of molecular routes in the initiation and progression of cancer. The c-Met acts

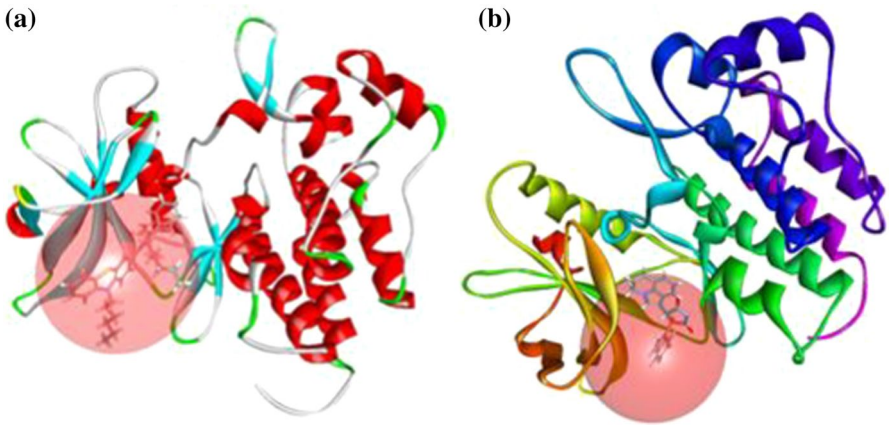

Fig. 18 Key flexible docked compound HHDIP in the active site of 3F66 **(a)** and key flexible docked compound of standard drug (tivantinib) in the active site of 3F66 **(b)**

as an (HGF) hepatocyte growth factor and mediates epithelial tissue remodeling, migration, morphogenesis, cell growth, differentiation and angiogenesis [73–76]. Moreover, in 2011, c-Met was found a sign of pancreatic cancer stem cell, which made it a suitable therapeutic target for cancer treatment [77].

In this study, against c-Met kinases protein target, the substrate-binding domain (SBD) site sphere of 3D flexible docked ligands such as HHDIP and standard drug, namely tivantinib, with the active site of 3F66 and its outcomes are shown in Fig. 18. The title molecule exhibited higher binding interaction energy of − 64.494(KCal/mol) against the target protein (3F66) and formed interaction with the amino acid of MET1160 (N–H….O; bond angle of 2.7Å). Standard anticancer drugs, namely tivantinib, interacted with the amino acids of ASN-1167 (N–H….O; 2.5Å) and ILE-1084 (C–H…O; 2.5Å) which also showed the binding interaction of -57.804 (KCal/mol) against the target 3F66. These compounds in silico section outcomes are shown in Table 11, and thereof hydrogen-bond interaction and 2D interactions are shown in Figs. 19 and 20.

In silico ADMET and toxicity profiles

The synthesized title compound from the current study exhibited superior absorption capacity (> 90% absorbed), as located within the ellipse. The graphical representation of HHDIP is presented in Fig. 21. In ADMET (adsorption, distribution, metabolisms, excretion and toxicity) analysis, HIA (human intestinal absorption), level of aqueous solubility, BBB (brain–blood barrier) penetration levels and CYP2D6 inhibiting values of this HHDIP were analyzed. The measurement of hepatotoxicity is able to predict its ADMET properties of molecules [78]. The title molecule was determined by a minimum range of solubility and exhibited a higher level of BBB penetration (Table 12). The important prediction of the toxicity profile of HHDIP using TOPKAT was also utilized in the range of QSTR quantitative

Table 11 Molecular docking results of HHDIP and standard drug tivantinib

Ligand name	CDocker energy	CDocker interaction energy	LibDock score	LibDock pose	Binding energy	Hydrogen bond interaction	Distance (Å)
HHDIP	10.346	48.868	59.867	9	**−64.493**	[MET1160]N–H…O	2.7
Standard drug Tivantinib PubChem ID – 11494412	11.648	27.868	79.106	88	−57.804	[ASN1167]N–H….O	2.5
						C–H…O[ILE1084]	2.5

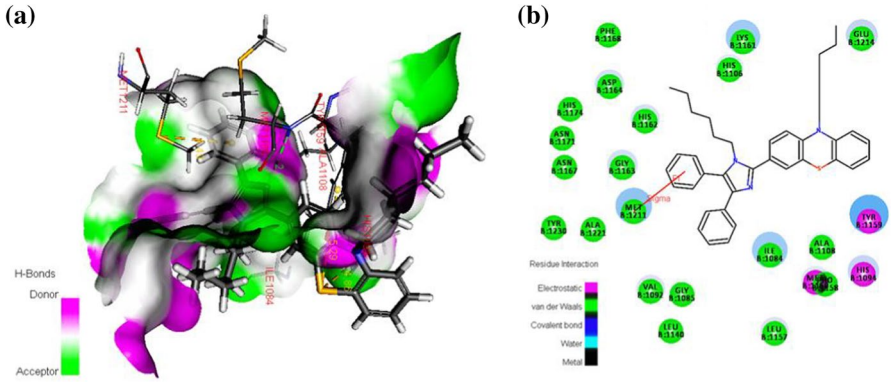

Fig. 19 High binding energy of H-bond interaction of (HHDIP) **(a)** and 2D image of compound (HHDIP) **(b)** in the active site of 3F66

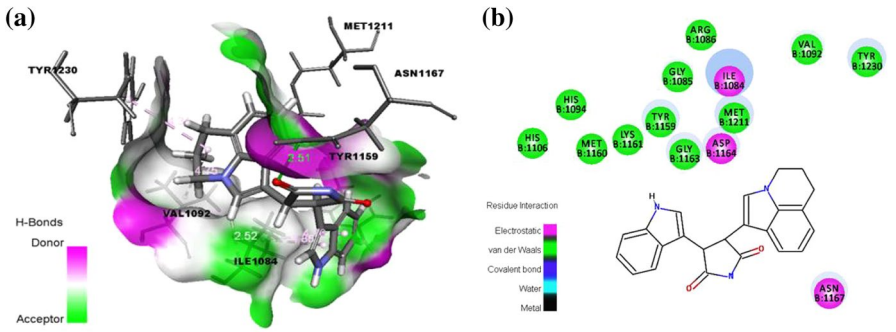

Fig. 20 Standard drug (tivantinib) receptor side interaction **(a)** and 2D image of standard drug **(b)** in the active site of 3F66

structure–toxicity relationship prototypes for a measure in unique toxicological assessment criteria such as developmental toxicity prediction, aerobic biodegradability, mutagenicity, skin irritation test. The prediction outcomes of ADMET-TOX showed leading optimization [79]. The compound, namely HHDIP, is nonmutagenic in AMES mutagenicity screening and shows mild ocular irritancy and noncarcinogenic property in nature (Table 13).

Conclusion

In the present study, the new compound HHDIP was synthesized and characterized using several analytical techniques, such as FTIR, UV–Vis spectroscopy, ^{1}H, and ^{13}C NMR, mass spectrum and elemental (CHNS/O) analysis. The structure of

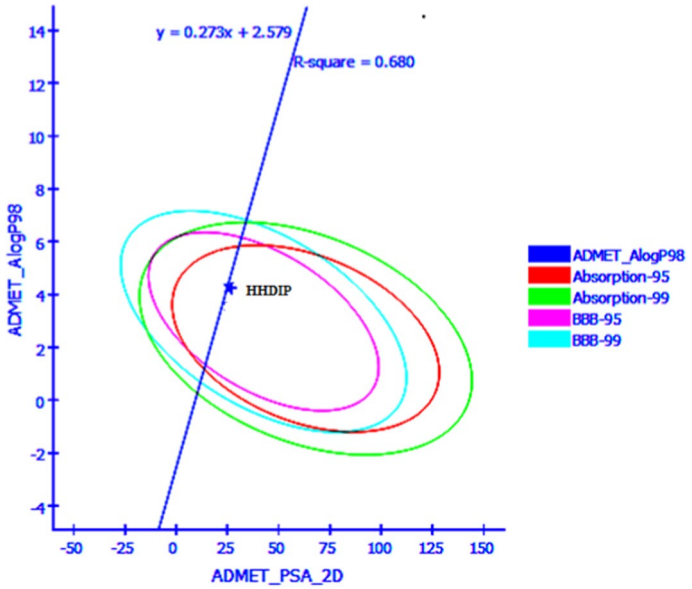

Fig. 21 Graphical representation of ADMET properties of HHDIP

Table 12 ADMET pharmacokinetic properties of HHDIP

Ligand name	Solubility level	Absorption level	BBB level	CYP2D6	Hepatotoxic	PPB	AlogP98	PSA-2D
HHDIP	2	0	0	−5.4679	4.15922	9.40543	4.241	26.287

HHDIP optimized molecular geometry, vibrational frequency and NMR chemical shifts of the compound were theoretically calculated using the DFT method, and comparison was completed with their well-matching experimental outcomes. The energies of essential molecular orbitals and the electronic absorption wavelengths of the analyzed molecule are also studied by the TD-DFT method besides the other electronic properties. The computed first-order hyperpolarizability (β), dipole moment (μ) and linear polarizability (α) of HHDIP were obtained to be larger than those of standard NLO material urea. Hence, HHDIP possesses large NLO optical property. The charge distribution of HHDIP was studied using the Mulliken population analysis. The FMOs (frontier molecular orbitals) were

Table 13 Toxicity profile of HHDIP using toxicity prediction—extensible protocol in Accelrys Discovery studio 4.0

Ligand name	AMES Mutagenicity	Development toxicity potential	Ocular irritancy	Skin irritancy	Skin sensitization	Carcinogenicity			
						Female mouse	Male mouse	Female rat	Male rat
HHDIP	Nonmutagenic	Toxic	Mild	None	None	Noncarcinogenic	Noncarcinogenic	Noncarcinogenic	Noncarcinogenic

calculated and showed HOMO–LUMO energy gap value of 4.0203 eV. In DFT chemical reactivity study, HHDIP showed lower softness HOMO–LUMO value of 2.2099. The computed thermodynamic properties were completed for this title compound; furthermore, the biological study of HHDIP showed outstanding anticancer activity. This compound also had significant interaction energy values against c-Met kinase protein target almost near to standard drug tivantinib, and it also possessed desirable pharmacokinetic properties. Future studies are exploring the promising anticancer property of this compound.

Acknowledgements The authors are delighted to thank LIFE (Loyola Institute of Frontier Energy) for supporting this study by providing with us laboratory facilities, instrumental facilities and infrastructural facilities. Also thanks to Plant Biology & Biotechnology department, Loyola College (Autonomous), for providing the laboratory facilities of in vitro studies and the Department of Chemistry, Saveetha Engineering College, Thandalam, for supporting this work.

Compliance with ethical standards

Conflict of interest The authors have no conflict of interest.

References

1. N.P. Desai, V. Trieu, L.Y. Hwang, R. Wu, P. Soon-Shiong, W.J. Gradishar, Anticancer Drugs **19**, 899 (2008)
2. A. Verma, S. Joshi, D. Singh, J. Chem. 2013 (2013)
3. C. Congiu, M.T. Cocco, V. Onnis, Bioorg. Med. Chem. Lett. **18**, 989 (2008)
4. I.R. Siddiqui, P.K. Singh, V. Srivastava, J. Singh, Indian J. Chem. **49B**, 512 (2010)
5. B. Narasimhan, D. Sharma, P. Kumar, Med. Chem. Res. **20**, 1119 (2011)
6. G. Roman, J.G. Riley, J.Z. Vlahakis, R.T. Kinobe, J.F. Brien, K. Nakatsu, W.A. Szarek, Bioorg. Med. Chem. **15**, 3225 (2007)
7. M.A. Babizhayev, Life Sci. **78**, 2343 (2006)
8. P.G. Nantermet, J.C. Barrow, S.R. Lindsley, M. Young, S.S. Mao, S. Carroll, C. Bailey, M. Bosserman, D. Colussi, D.R. McMasters, J.P. Vacca, Bioorg. Med. Chem. Lett. **14**, 2141 (2004)
9. D. Sharma, B. Narasimhan, P. Kumar, V. Judge, R. Narang, E. De Clercq, J. Balzarini, Eur. J. Med. Chem. **44**, 2347 (2009)
10. J.R. Kuma, Pharmacophore. **1**, 167 (2010)
11. H. Bendaha, L. Yu, R. Touzani, R. Souane, G. Giaever, C. Nislow, C. Boone, S. El Kadiri, G.W. Brown, M. Bellaoui, Eur. J. Med. Chem. **46**, 4117 (2011)
12. H.M. Alkahtani, A.Y. Abbas, S. Wang, Bioorg. Med. Chem. Lett. **22**, 1317 (2012)
13. H. Eshghi, M. Rahimizadeh, M. Hasanpour, M. Bakavoli, Res. Chem. Intermed. **41**, 4187 (2015)
14. Y. Fang, R. Yuan, W.H. Ge, Y.J. Wang, G.X. Liu, M.Q. Li, J.B. Xu, Y. Wan, S.L. Zhou, X.G. Han, P. Zhang, Res. Chem. Intermed. **43**, 4413 (2017)
15. Y.T. Liu, X.M. Sun, D.W. Yin, F. Yuan, Res. Chem. Intermed. **39**, 1037 (2013)
16. S.M. Abu-Bakr, F.A. Bassyouni, M.A. Rehim, Res. Chem. Intermed. **38**, 2523 (2012)
17. S. Zhou, F. Li, P. Zhang, L. Jiang, Res. Chem. Intermed. **39**, 1735 (2013)
18. M.J. Frisch, G.W. Trucks, H.B. Schlegel, G.E. Scuseria, M.A. Robb, J.R. Cheeseman, G. Scalmani, V. Barone, B. Mennucci, G.A. Petersson, H. Nakatsuji, M. Caricato, X. Li, H.P. Hratchian, A.F. Izmaylov, J. Bloino, G. Zheng, J.L. Sonnenberg, M. Hada, M. Ehara, K. Toyota, R. Fukuda, J. Hasegawa, M. Ishida, T. Nakajima, Y. Honda, O. Kitao, H. Nakai, T. Vreven, J.A. Montgomery Jr., J.E. Peralta, F. Ogliaro, M. Bearpark, J.J. Heyd, E. Brothers, K.N. Kudin, V.N. Staroverov, R. Kobayashi, J. Normand, K. Raghavachari, A. Rendell, J.C. Burant, S.S. Iyengar, J. Tomasi, M. Cossi, N. Rega, J.M. Millam, M. Klene, J.E. Knox, J.B. Cross, V. Bakken, C. Adamo, J. Jaramillo, R. Gomperts, R.E. Stratmann, O. Yazyev, A.J. Austin, R. Cammi, C. Pomelli, J.W. Ochterski, R.L.

Martin, K. Morokuma, V.G. Zakrzewski, G.A. Voth, P. Salvador, J.J. Dannenberg, S. Dapprich, A.D. Daniels, O. Farkas, J.B. Foresaman, J.V. Ortiz, J. Cioslowski, D.J. Fox, Gaussian Inc., Wallingford CT. **121**, 150 (2009)
19. Z. Özer, J. Iran. Chem. Soc. **10**, 1 (2020)
20. C. Lee, W. Yang, R.G. Parr, Phys. Rev. B. **37**, 785 (1988)
21. H.B. Schlegal, J. Comput. Chem. **3**, 214 (1982)
22. P.J. Stevens, J.F. Devlin, J.F. Chabalowski, M.J. Frisch, J. Phys. Chem. **98**, 11623 (1994)
23. L.D. Popov, S.I. Levchenkov, I.N. Shcherbakov, G.G. Aleksandrov, Y.P. Tupolova, V.V. Lukov, O.I. Askalepova, V.A. Kogan, J. Struct. Chem. **54**, 619 (2013)
24. J.I. Ahamed, M. Priya, P. Vinothkumar, K. Sathyamoorthy, P. MuraliManohar, J. Liu, M.F. Valan, J. Mol. Struct. **1202**, 127241 (2020)
25. A. Frisch, A.B. Neilson, A.J. Holder, Pittsburgh, PA. 566 (2000)
26. R.F.W. Bader, *A Quantum Theory* (Clarendon, Oxford, 1990)
27. R. Bauernschmitt, R. Ahlrichs, Chem. Phys. Lett. **256**, 454 (1996)
28. E. Kose, A. Atac, M. Karabacak, C. Karaca, M. Eskici, A. Karanfil, Spectrochim. Acta A. **97**, 435 (2012)
29. R. Ditchfield, J. Chem. Phys. **56**, 5688 (1972)
30. J. Koska, V.Z. Spassov, A.J. Maynard, L. Yan, N. Austin, P.K. Flook, C.M. Venkatachalam, J. Chem. Inf. Model. **48**, 1965 (2008)
31. M. Arshad, J. Iran. Chem. Soc. **1**, 11 (2020)
32. V.Z. Spassov, P.K. Flook, L. Yan, Protein Eng. Des. Sel. **21**, 91 (2008)
33. M. Karabacak, S. Bilgili, A. Atac, Spectrochim. Acta A. **150**, 83 (2015)
34. K. Yakushi, I. Ikemoto, H. Kuroda, Acta Cryst. B. **30**, 1738 (1974)
35. Y. Wang, S. Saebar, C.U. Pittman, J. Mol. Struct. (Theochem). **281**, 91 (1993)
36. K. Yakushi, I. Ikemoto, H. Kuroda, Acta Cryst. B. **27**, 1710 (1971)
37. N.M. O'Boyle, A.L. Tenderholt, K.M. Langner, J. Comput. Chem. **29**, 839 (2008)
38. D. Zhao, K.D. Doney, H. Linnartz, J. Mol. Struct. **296**, 1 (2014)
39. H. Tanak, Y. Köysal, Y. Ünver, M. Yavuz, S. Isık, K. Sancak, Mol. Phys. **108**, 127 (2010)
40. S. Sevvanthi, S. Muthu, M. Raja, J. Mol. Struct. **1173**, 251 (2018)
41. P.J. Brimmer, P.R. Griffiths, Appl. Spectrosc. **42**, 242 (1988)
42. S. Sakthivel, T. Alagesan, S. Muthu, C.S. Abraham, E. Geetha, J. Mol. Struct. **1156**, 645 (2018)
43. P.J. Larkin, M.P. Makowski, N.B. Colthup, Spectrochim. Acta A **55**, 1011 (1999)
44. S. Muthu, E.I. Paulraj, Solid State Sci. **14**, 476 (2012)
45. M. Silverstein, G.C. Basseler, C. Morill, Wiley, New York. (1981)
46. V. Krishnakumar, R. Ramasamy, Indian J. Pure Appl. Phys. **40**, 252 (2002)
47. C.S. Hsu, Spectrosc. Lett. **7**, 439 (1974)
48. B.B. Snider, M.V. Busuyek, Tetrahedron **57**, 3301 (2001)
49. X. Gao, W. Jiang, G. Jiménez-Osés, M.S. Choi, N.K. Houk, Y.T. Christopher, T. Walsh, Chem. Biol. **20**, 870 (2013)
50. S. Karabuga, S.L. Bars, I. Karakaya, S. Gumus, Tetrahedron Lett. **56**, 101 (2015)
51. N.B. Patel, J.C. Patel, Arab. J. Chem. **4**, 403 (2011)
52. D. Sajan, I.H. Joe, V.S. Jayakumar, J. Zaleski, J. Mol. Struct. **785**, 43 (2006)
53. A. Ben Ahmed, N. Elleuch, H. Feki, Y. Abid, C. Minot, Spectrochim. Acta A. **79**, 554 (2011)
54. S. Muthu, E.E. Porchelvi, M. Karabacak, A.M. Asiri, S.S. Swathi, J. Mol. Struct. **1081**, 400 (2015)
55. G. Vengatesh, M. Sundaravadivelu, Res. Chem. Intermed. **45**, 4395 (2019)
56. M. Raja, R.R. Muhamed, S. Muthu, M. Suresh, J. Mol. Struct. **1128**, 481 (2017)
57. S.M. Hiremath, A. Suvitha, N.R. Patil, C.S. Hiremath, S.S. Khemalapure, S.K. Pattanayak, V.S. Negalurmath, K. Obelannavar, S.J. Armaković, S. Armaković, Spectrochim. Acta A. **205**, 95 (2018)
58. N. Subramanian, N. Sundaraganesan, J. Jayabharathi, Spectrochim Acta A. **76**, 259 (2010)
59. B. Ferah, Anadolu Üniversitesi Bilim Ve Teknoloji Dergisi-B Teorik Bilimler **4**, 74 (2016)
60. G. Gece, Corrosion Sci. **50**, 2981 (2008)
61. D.F.V. Lewis, C. Ioannides, D.V. Parke, Xenobiotica **24**, 401 (1994)
62. R.G. Pearson, Proc. Natl. Acad. Sci. **83**, 8440 (1986)
63. B. Fathima Rizwana, J.C. Prasana, S. Muthu, Int. J. Mater. Sci. **12**, 196 (2017)
64. A. Pradhan, S. Vishwakarma, Chem. Int. **6**, 224 (2020)
65. A. Viji, V. Balachandran, S. Babiyana, B. Narayana, V.V. Saliyan, J. Mol. Struct. **1203**, 127452 (2020)

66. F. Blanco, I. Alkorta, J. Elguero, Magn. Reson. Chem. **45**, 797 (2007)
67. K. Pihlaja, E. Kleinpeter, Wiley, Hoboken, 17 (1994)
68. S.C. Yavuz, S. Akkoç, E. Sarıpınar, Synth. Commun. **49**, 3198 (2019)
69. M.R. Saberi, T.K. Vinh, S.W. Yee, B.N. Griffiths, P.J. Evans, C. Simons, J. Med. Chem. **49**, 1016 (2006)
70. B. Venkatadri, A. Khusro, C. Aarti, M.R. Rameshkumar, P. Agastian, Asian. Pac. J. Trop. Biomed. **7**, 782 (2017)
71. T. Hatano, H. Kagawa, T. Yasuhara, T. Okuda, Chem. Pharm. Bull. **36**, 2090 (1988)
72. V. Suresh, N. Senthilkumar, R. Thangam, M. Rajkumar, C. Anbazhagan, R. Rengasamy, P. Gunasekaran, S. Kannan, P. Palani, Process Biochem. **48**, 364 (2013)
73. A.Y. Elnagar, P.W. Sylvester, K.A. El Sayed, Planta Med. **77**, 1013 (2011)
74. W. Tai, T. Lu, H. Yuan, F. Wang, H. Liu, S. Lu, Y. Leng, W. Zhang, Y. Jiang, Y. Chen, J. Mol. Model. **18**, 3087 (2012)
75. C.R. Maroun, T. Rowlands, Pharmacol. Ther. **142**, 316 (2014)
76. L. Ye, X. Ou, Y. Tian, B. Yu, Y. Luo, B. Feng, H. Lin, J. Zhang, S. Wu, Eur. J. Med. Chem. **65**, 112 (2013)
77. C. Li, J.J. Wu, M. Hynes, J. Dosch, B. Sarkar, T.H. Welling, M.P. di Magliano, D.M. Simeone, Gastroenterology **141**, 2218 (2011)
78. P. Daisy, S. Suveena, Asian J. Pharm. Clin. Res. **5**, 149 (2012)
79. M. Jayakanthan, G. Wadhwa, T.M. Mohan, L. Arul, P. Balasubramanian, D. Sundar, Lett. Drug. Des. Discov. **6**, 14 (2009)

Affiliations

J. Irshad Ahamed[1] · Mariamichael F. Valan[1] · Kamalarajan Pandurengan[2] · Paul Agastian[3] · Babu Venkatadri[3] · Marimuthu R. Rameshkumar[4] · Kandaswamy Narendran[5]

✉ J. Irshad Ahamed
irshad@loyolacollege.edu

[1] Department of Chemistry, LIFE (Loyola Institute of Frontier Energy), Loyola College, University of Madras, Nungambakkam, Chennai, Tamil Nadu, 600034, India

[2] Department of Science and Humanities, R.M.D Engineering College, Kavaraipettai, Tamil Nadu 601206, India

[3] Department of Plant Biology and Biotechnology, Loyola College (Autonomous), University of Madras, Chennai, Tamil Nadu, 600 034, India

[4] Infectious Diseases Laboratory, YR Gaitonde Centre for AIDS Research and Education, Voluntary Health Services Hospital Campus, Chennai, Tamil Nadu 600 113, India

[5] Department of Chemistry, Saveetha Engineering College, Thandalam, Chennai 602 105, India